Response of small intestinal epithelial cells to acute disruption of cell division through CDC25 deletion

Gwanghee Lee[a], Lynn S. White[a,d], Kristen E. Hurov[a,d,1], Thaddeus S. Stappenbeck[b], and Helen Piwnica-Worms[a,c,d,2]

[a]Departments of Cell Biology and Physiology, [b]Pathology and Immunology, and [c]Internal Medicine and [d]Howard Hughes Medical Institute, Washington University School of Medicine, St. Louis, MO 63110

Communicated by Emil R. Unanue, Washington University School of Medicine, St. Louis, MO, January 23, 2009 (received for review October 30, 2008)

The CDC25 protein phosphatases (CDC25A, B, and C) drive cell cycle transitions by activating key components of the cell cycle engine. CDC25A and CDC25B are frequently overproduced in human cancers. Disruption of *Cdc25B* or *Cdc25C* individually or in combination has no effect on mouse viability. Here we report that CDC25A is the only family member to provide an essential function during early embryonic development, and that other family members compensate for its loss in adult mice. In contrast, conditional disruption of the entire family is lethal in adults due to a loss of small intestinal epithelial cell proliferation in crypts of Lieberkühn. *Cdc25* loss induced Wnt signaling, and overall crypt structures were preserved. In the face of continuous Wnt signaling, nearly all crypt epithelial progenitors differentiated into multiple cell lineages, including crypt base columnar cells, a proposed stem cell. A small population of Musashi/Dcamkl-1/nuclear β-catenin–positive epithelial cells was retained in these crypts. These findings have implications for the development of novel, less cytotoxic cancer chemotherapeutic drugs that specifically target the cell cycle.

CDC25 phosphatases | cell cycle | stem cells

The CDC25 phosphatases promote cell cycle progression by activating cyclin-dependent protein kinases (1–6). In mice, *Cdc25A*, *B*, and *C* exhibit overlapping but distinct patterns of expression during development and in adult tissues (7–10). This suggests that they have distinct biological functions in embryonic and adult mice. Mice lacking CDC25B and CDC25C, individually or in combination, are viable and develop normally, and embryonic fibroblasts derived from these mice exhibit normal cell cycle parameters in culture (11–13). These findings demonstrate that mice can survive throughout embryogenesis and adulthood with a single member of the family, CDC25A. Here we report the consequences of deleting *Cdc25A* alone and in combination with *Cdc25B* and *Cdc25C* in mice. Our data demonstrate that CDC25A provides an essential function during early embryogenesis, and that CDC25B and/or CDC25C compensate for CDC25A loss in adult mice. In contrast, mice lacking all 3 CDC25s die within 1 week due to complete loss of epithelial cell proliferation in the small intestinal crypts.

We used this model to explore how small intestine stem and progenitor cells respond to the acute disruption of cell division. The self-renewing epithelium of the adult small intestine contains tetrapotent stem cells that give rise to rapidly proliferating committed daughter cells, which in turn produce terminally differentiated cells (14). One of these lineages, Paneth cells, are located in crypts of Lieberkühn along with stem and progenitor cells. Analysis of gene expression and cellular morphology, as well as lineage tracing experiments, suggest that stem cells are intermingled with or lie just above Paneth cells at the crypt base (15–18). These stem cells are considered to provide the source of recovery after damage to the epithelial lining from such factors as irradiation and chemotherapeutic agents. We report that CDC25 loss acutely disrupts epithelial cell proliferation in the small intestines of mice. This leads to a concomitant increase in canonical Wnt signaling, which in turn functions to maintain crypt architecture and induce differentiation of most crypt progenitor cells, with the exception of those cells residing immediately above the Paneth cell compartment. This study is the first to assess the consequences of conditionally deleting an entire family of positive cell cycle regulators (the CDC25 family) in adult mice. As such, our findings are likely to predict phenotypes that can be expected when other families of positive cell cycle regulators are combinatorially deleted in mice.

Results

CDC25A Is Essential for Early Embryonic Development. Because simultaneous deletion of *Cdc25B* and *Cdc25C* is known to have no effect on mouse viability or cell cycle parameters (13), we used a gene targeting strategy to disrupt the remaining family member (*Cdc25A*). Null and floxed alleles of *Cdc25A* were generated by a standard protocol [supporting information (SI) Fig. S1]. Cumulative genotyping of 519 offspring from heterozygous crosses revealed 162 WT mice, 357 heterozygous mutant mice, and 0 homozygous mutant mice (Table 1). The mice heterozygous for *Cdc25A* were viable, fertile, and healthy, demonstrating that a single allele of *Cdc25A* is sufficient for normal mouse development (Table 1). In contrast, mice homozygous for the mutation were never identified, indicating that the *Cdc25A* null mutants died in utero. Blastocysts [embryonic day 3.5 (E3.5)] from intercrosses between $Cdc25A^{+/-}$ mice were genotyped. The expected number of *Cdc25A* null blastocysts was determined (Table 1), and blastocysts homozygous for the targeted mutation of *Cdc25A* were morphologically normal (Fig. S2*B*). Thus, targeted disruption of *Cdc25A* did not appear to negatively affect preimplantation development.

To determine the precise time of death of *Cdc25A* null embryos, laser capture microdissection (LCM) was used to genotype E5.5–E7.5 embryos (Table 1). At E7.5, both WT and heterozygous embryos displayed normal growth and development. In contrast, 3 *Cdc25A* null embryos exhibited severe growth and morphological abnormalities by E7.5 (Fig. S2*A*, *Top Right*). Seven empty decidua were seen, indicating that most of the *Cdc25A* null embryos were resorbed by this time. TUNEL staining revealed significant apoptosis in *Cdc25A* null embryos by E7.5 (Fig. S2*A*, *Bottom Right*). At E6.5, 12 resorbed deciduas and 1 phenotypically normal *Cdc25A* null embryo were found (data not shown). Apoptosis was not observed in this latter embryo (data not shown), indicating that embryos lacking CDC25A can occasionally survive to E6.5. In summary, our findings indicate that CDC25A-deficient embryos exhibit growth retardation and die before E7.5 through an apoptotic pathway.

Author contributions: G.L., K.E.H., T.S.S., and H.P.-W. designed research; G.L. and L.W. performed research; G.L., L.W., K.E.H., and T.S.S. contributed new reagents/analytic tools; G.L., T.S.S., and H.P.-W. analyzed data; and G.L., T.S.S., and H.P.-W. wrote the paper.

The authors declare no conflict of interest.

[1]Current address: Department of Genetics, Harvard Partners Center for Genetics and Genomics, Harvard Medical School, 77 Avenue Louis Pasteur, Boston, MA 02115.

[2]To whom correspondence should be addressed. E-mail: hpiwnica@cellbiology.wustl.edu.

This article contains supporting information online at www.pnas.org/cgi/content/full/0900751106/DCSupplemental.

Table 1. Genotype analysis of progeny from *Cdc25A*$^{+/-}$ intercrosses

	+/+	+/−	−/−	Empty/ Resorbed	Undetermined
Pups born	162	357	0	NA	0
E8.5	6	9	*1	4	0
E7.5	6	7	*3	7	0
E6.5	22	15	1	12	16
E5.5	1	5	0	5	4
Blastocysts (E3.5)	17	45	16	NA	0

NA, not applicable.
*Abnormal morphology.

***Cdc25A*$^{-/-}$ Blastocysts Fail to Expand Their Inner Cell Mass When Cultured In Vitro.** Blastocysts of all 3 genotypes from intercrosses between *Cdc25*$^{+/-}$ were able to hatch, attach to the culture dish, and give rise to adherent sheets of trophoblastic giant cells. *Cdc25A* null blastocysts were unable to expand their inner cell mass, however (Fig. S2*B*). These findings are consistent with those obtained in vivo, demonstrating that *Cdc25A* null embryos can hatch and implant normally but have defective postimplantation development.

***Cdc25A* Is Disrupted in Adult Mice.** To determine whether CDC25A is required in adult mice, we used an inducible Cre-loxP targeting strategy to conditionally delete *Cdc25A* in all tissues of the adult mouse (19). All major organs in the *R26CreER*^{T};*A*$^{f/-}$*BCKO* mice were histologically indistinguishable from those in WT mice (data not shown). These findings demonstrate that insertion of the *loxP* sites per se did not impair *Cdc25A* expression.

We injected 4-hydroxy-tamoxifin (OHT) i.p. for 3 consecutive days to generate mice globally deleted for *Cdc25A* (AKO) or for all 3 *Cdc25* family members (TKO). We also injected control littermates with OHT. The deletion frequency (i.e., conversion of floxed to null allele) varied from 46% to 92% in various organs of the AKO and TKO mice, and quantitative RT-PCR (qRT-PCR) revealed a ≈95% reduction in *Cdc25A* mRNA levels in the small intestine of the AKO and TKO mice relative to control (WT) mice (Fig. S3 *A* and *B*). The AKO mice survived and did not exhibit the phenotypes observed in the TKO mice (see below).

The Small Intestine Is Significantly Shortened in TKO Mice. Within 1 week of the first OHT injection, the TKO mice died, exhibiting significant (20%) loss of body weight. The small intestine, but not the large intestine, was shortened significantly (by 40%) in the TKO mice (Fig. 1*A*). This phenotype did not exist before OHT injection, as demonstrated by the fact that small intestine length did not differ between the *R26CreER*^{T};*A*$^{f/-}$*BCKO* mice and controls (Fig. S4). Small intestine length did not differ significantly between OHT-injected AKO and control mice (Fig. 1*A*). The Cre-mediated deletion of the floxed *Cdc25A* allele in the small intestine of OHT-treated *R26CreER*^{T};*A*$^{f/-}$ mice was comparable to that in *R26CreER*^{T};*A*$^{f/-}$*BCKO* mice (Fig. S3*A* and *B*). Furthermore, recombination at the *Cdc25A* locus remained high after 13 months of the first OHT injection, demonstrating that the lack of a phenotype in the AKO mice was not due to the proliferation of cells in which Cre expression failed to disrupt the *Cdc25A* locus (Fig. S3*C*). As additional controls, WT littermates injected with OHT demonstrated no significant differences in small intestine length (Fig. 1*A*).

Homeostasis Is Lost in the Small Intestine of TKO Mice. The TKO mice demonstrated a significant loss of small intestinal villus height (Fig. 1*B*). In proximal regions, the shortened villi of the TKO mice were lined by shorter, less-dense enterocytes (compare the insets in Fig. 1*C*). Distal villi were shortened significantly and demonstrated focal areas of complete loss (data not shown). The effect on villus height was specific for the TKO mice; the AKO mice showed no significant differences in villus height after OHT injection (Fig. 1*B* and *D*).

The diminished small intestinal villus height in the TKO mice suggests a loss of cell production from the underlying crypts. Examination of the crypts revealed profound atrophy in the TKO

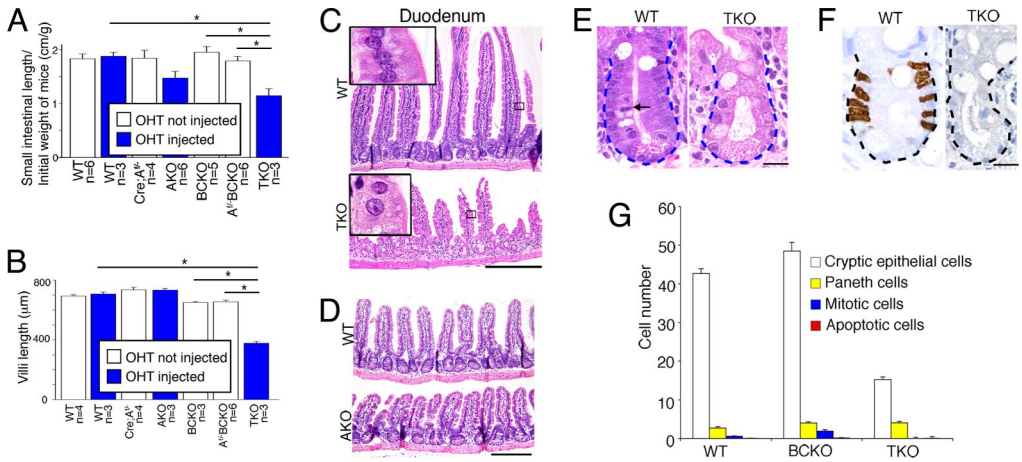

Fig. 1. Loss of homeostasis in small intestines of TKO mice. All graphical data are presented as mean ± SEM. An asterisk indicates a significant difference from WT mice injected with OHT as determined by the 2-tailed Student *t*- test. The α level is .05. Individual *P* values are presented in each panel. (*A*) Significant shortening of the small intestine in TKO mice. From the top, *P* values are .008, .003, and .004. Intestinal lengths did not vary significantly between the AKO mice and the WT mice ($P = .07$). (*B*) Significant shortening of villi in the small intestine of TKO mice. From the top, *P* values are .0004, .008, and .0001. (*C*) Shortened villi in the small intestine of TKO mice. (Scale bar: 0.5 mm.) The insets show higher magnifications of boxed areas. (*D*) Lack of phenotype in the small intestine of mice disrupted for *Cdc25A*. The mice were killed 90 days after the final OHT injection. (*E*) Absence of mitotic figures in crypt cells of TKO mice. (Scale bar: 20 μm.) Crypt borders are depicted with blue hatched lines. (*F*) Absence of BrdU-positive cells in crypts of TKO mice. (Scale bar: 20 μm.) Crypt borders are depicted with black hatched lines. (*G*) Crypts within the proximal portion of the small intestine of OHT mice were examined for epithelial cells, Paneth cells, mitotic cells (presence of mitotic figures), and apoptotic cells (presence of fragmented nuclei). Areas containing Brunner's gland were excluded from analysis. Twenty crypts were counted per mouse, and 2 mice of each genotype were evaluated. Similar patterns were observed in mid and distal portions of the small intestine (data not shown).

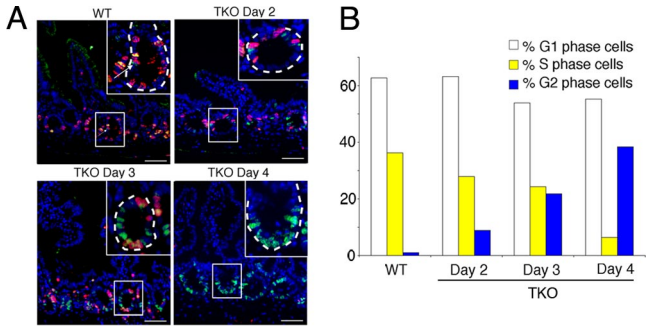

Fig. 2. G1 and G2 cell cycle arrest of epithelial cells in the small intestine of TKO mice. (*A*) Loss of CDC25 causes intestinal epithelial cells to arrest in the G1 and G2 phases of the cell cycle. *R26CreER^{T};A^{fl-}BCKO* mice were injected with OHT for 1, 2, or 3 days and killed 24 h after the last injection to generate TKO mice. One hour before sacrifice, the mice were injected with BrdU to label S-phase cells. Green, geminin; red, BrdU; blue, DAPI. Insets display individual crypts at higher magnifications. Crypt borders are depicted with white hatched lines. The arrow in the WT image denotes a G2 cell in the crypt. (Scale bar: 10 μm.) (*B*) G1-, S-, and G2-phase cells were quantitated from the images shown in (*D*). Total nuclei counted: WT, 502; TKO, 416 on day 2, 399 on day 3, and 409 on day 4.

intestines (Fig. 1*E*–*G*). Interestingly, the overall depth of the TKO crypts was decreased only modestly, whereas crypt width was reduced more appreciably. The crypts of the TKO mice were 47% smaller than those in the BCKO control mice (Fig. S5). The diminished volume of the TKO crypts corresponded to a 70% decrease in the total number of epithelial cells per crypt. Interestingly, the number of mature Paneth cells per crypt was the same in the TKO mice and the controls, indicating a specificity of epithelial cell loss in the TKO mice (Fig. 1*G*), which suggests that the major effect is on epithelial stem cells and progenitor cells.

G1 and G2 Cell Cycle Arrest of Epithelial Cells in the Small Intestine of TKO Mice. We next explored the cause of epithelial cell loss. The crypt compartments of the TKO mice contained virtually no M-phase cells (Fig. 1*E* and *G*) and only few BrdU-positive cells (Fig. 1*F*). Conversely, the TKO crypts did not exhibit an increased number of apoptotic cells (Figs. 1*E* and *G* and Fig. S6). These findings demonstrate that a lack of proliferation, not enhanced apoptosis, results in the dramatic phenotype observed in the small intestine of the TKO mice. We conducted a time course evaluation to determine the cell cycle stage at which intestinal epithelial cells are arrested (Fig. 2*A* and *B*). Small intestines were processed for immunohistochemistry with antibodies specific for geminin (S- and G2-phase marker) (20) and BrdU (S-phase marker). When *Cdc25A* was acutely disrupted in intestinal epithelial cells also lacking CDC25B and C, the percentage of S-phase cells decreased, the percentage of G2-phase cells increased, and the percentage of G1-phase cells did not change significantly (Fig. 2*A* and *B*). These findings indicate that in TKO mice, cells in the G1 phase of the cell cycle are arrested in G1, whereas cells in the S and G2 phases of the cell cycle are arrested in G2.

Crypt Structure and Composition in TKO Mice. We further examined small intestines from TKO and control (WT) mice using both light microscopy and electron microscopy (EM), to explore the effects of cell cycle arrest on epithelial progenitors that include both tetrapotent stem cells and their lineage-committed proliferative daughters. PAS/Alcian blue–stained sections of crypts from the WT mice (Figs. 3*A* and Fig. S6*A*–*C*) revealed mature

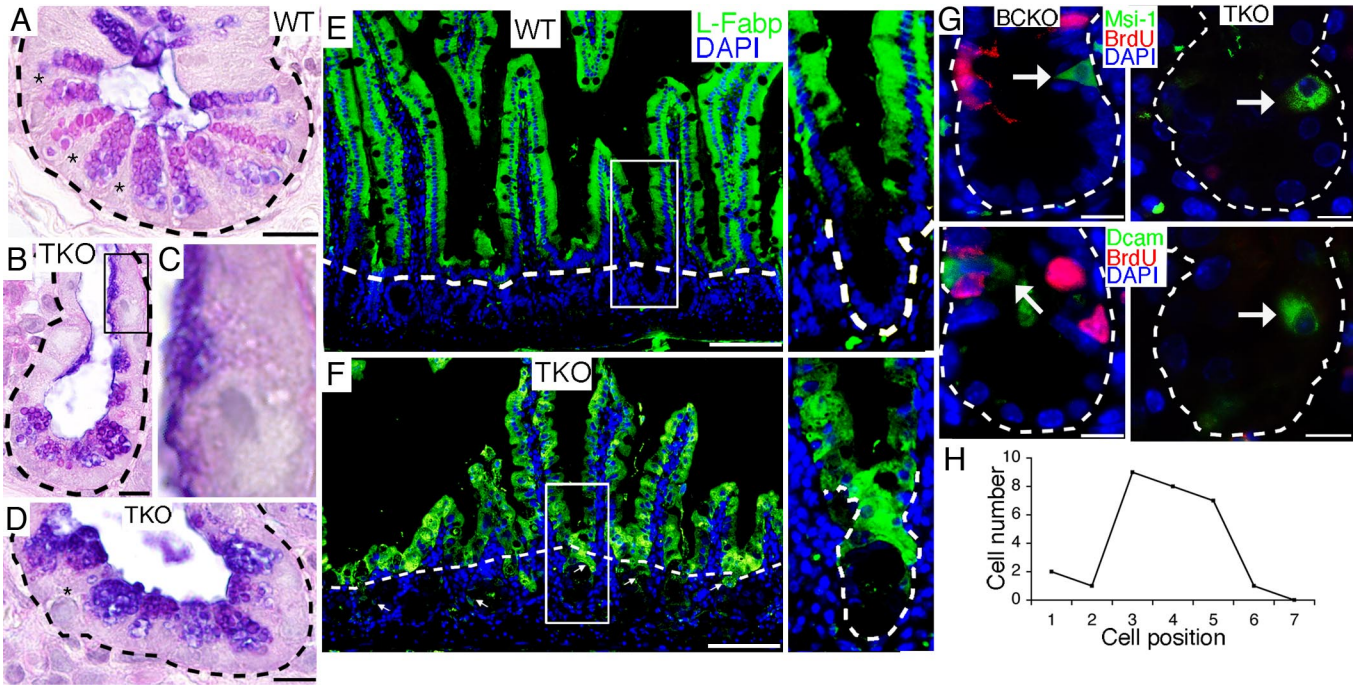

Fig. 3. Morphology and composition of intestinal crypts in TKO mice. (*A*–*D*) Intestinal sections were stained with PAS/Alcian blue to label Paneth cells and goblet cells. Sections from WT (*A*) and TKO (*B*–*D*) mice are shown. The inset in (*B*) is magnified in (*C*). In (*A*), asterisks indicate CBC cells. In (*D*), asterisks indicate immature Paneth cells. Crypt borders are indicated with black hatched line. (Scale bar: 10 μm.) (*E* and *F*) Intestinal sections were stained with the enterocyte-specific marker L-Fabp. Sections from WT (*E*) and TKO (*F*) mice are shown. Green, L-Fabp; blue, nuclei (DAPI). Hatched lines denote crypt margins. (Scale bar: 100 μm.) (*G*) Musashi-1– and Dcamkl-1–positive cells are maintained in TKO mice. Green (*Upper*), Musashi-1; green (*Lower*), Dcamkl-1; red, BrdU; blue, DAPI. (Scale bars: 20 μm.) Crypt borders are outlined. Arrows indicate cells staining negative for BrdU but positive for Musashi-1 or Dcamkl-1. (*H*) The number and location of 28 Mushashi-1–positive cells were determined in TKO mice. The cell at the base of the crypt was defined as position 1.

Paneth cells at the base of these structures, interspersed with granule-free crypt base columnar (CBC) cells. The middle and upper crypts contained occasional differentiated goblet cells, as well as granule/mucous-free columnar cells that represent lineage-committed proliferative precursors for differentiated epithelial cells.

Histological sections of TKO small intestinal crypts exhibited extensive premature differentiation along multiple epithelial lineages. PAS/Alcian blue–stained sections of TKO small intestines revealed mature Paneth cells at the crypt base (Figs. 3*B* and *D* and Fig. S7*D–G*); however, undifferentiated CBC cells were not identified in TKO crypts. In their place were cells with scattered, much smaller PAS/Alcian blue–positive apical granules, consistent with early Paneth cell differentiation (Fig. 3*D* and Fig. S6). The middle and upper crypts demonstrated extensive loss of lineage-committed precursor cells. In their place in the mid-crypts of TKO mice were epithelial cells containing small, mucin-containing apical thecas, consistent with early goblet cell differentiation (Fig. 3*C*). Epithelial cells in the upper crypt (Fig. 3*F*) were positive for markers of enterocytic differentiation, such as L-Fabp (21). This finding is in contrast to that in WT small intestines, where L-Fabp expression was restricted to epithelial cells that had exited the crypt (Fig. 3*E*). Thus, in the absence of proliferation, increased epithelial cell differentiation occurs along multiple lineages occurring in distinct locations within the crypts for each lineage.

We next investigated whether epithelial stem cells also underwent premature differentiation in the TKO mice. Two proposed positions of small intestinal epithelial stem cells are in a ring immediately above the Paneth cells (17, 18) and in the crypt base where CBC cells reside (15). Because CBC cells were not apparent in the TKO model, we evaluated the expression of Musashi-1 and Dcamkl-1 (proposed markers for intestinal epithelial stem cells), as well as a subset of early progenitors in an area immediately above Paneth cells (22, 23). Crypt cells staining negative for BrdU but positive for either Musashi-1 or Dcamkl-1 localized to the +4 to +6 crypt position in both control and TKO crypts (Fig. 3*G* and *H*).

The presence of epithelial cells containing potential stem cell markers suggests that canonical Wnt signaling was still occurring, because this pathway is required to maintain the self-renewal capacity of multipotent stem cells and for maturation of Paneth cells in intestinal crypts (24–26). We observed elevated expression of well-characterized Wnt targets, including *c-Myc* and *Dkk1*, 2 Tcf-4/β-catenin targets, as well as *Wnt 3* and *Wnt 9b*, in the small intestine of the TKO mice (Fig. S8). In addition, we found a ≈50% increase in the total number of cells per crypt staining positive for nuclear β-catenin in the TKO mice (Fig. 4*A* and *B*). Epithelial cells other than Paneth cells staining positive for nuclear β-catenin were present throughout the crypt, including cells in the +4 position. Cells staining positive for both nuclear β-catenin and Musashi-1 also were observed in the +4 position (Fig. S8 *H–J*). These findings demonstrate that the lack of proliferation due to loss of CDC25 led to enhanced Wnt signaling and concomitant differentiation of progenitors along multiple lineages in the small intestines of TKO mice, with the exception of cells residing immediately above the Paneth cell compartment.

EM analysis confirmed the effects of epithelial cell cycle arrest on differentiation (Fig. 4*C–G*). Both mature and immature Paneth cells were present in the crypt bases of the TKO mice (Fig. 4*E* and *G*). CBC cells were completely absent in the crypts of the TKO mice and were replaced by immature Paneth cells (Fig. 4*E* and *G*). The mid-crypts contained predominantly cells containing small amounts of apical mucin, consistent with the presence of immature goblet cells (Fig. 4*E*, arrow). The only granule-free cells in the mid-crypts were in a position above the Paneth cells (Fig. 4*E* and *F*), consistent with the position of

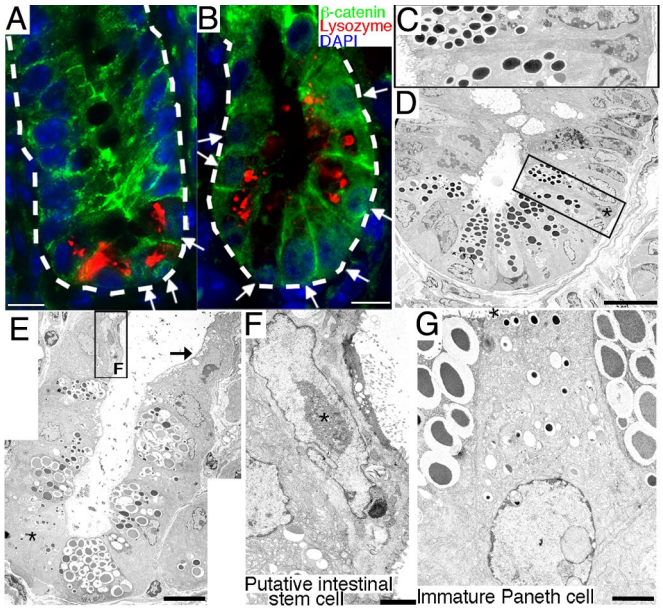

Fig. 4. Enhanced Wnt signaling and differentiation in crypts of TKO mice. (*A* and *B*) Tissue sections of small intestines prepared from WT (*A*) and TKO (*B*) mice were stained with antibodies specific for β-catenin (green) and lysozyme (red). Nuclei were stained with DAPI (blue). Arrows indicate cells staining positive for nuclear β-catenin. (Scale bar: 10 μm.) (*C–G*) Small intestines were dissected and processed for transmission electron microscopy. (*D*) An EM section of crypt from a WT mouse and higher magnification (*C*) showing a CBC cell between 2 mature Paneth cells, marked with an asterisk in (*D*). (*E*) EM sections of crypt from a TKO mouse. The inset in (*E*) is shown at higher magnification in (*F*). The arrow indicates an immature goblet cell with characteristic apical mucinogenic granules. In (*F*), a cell with stem-like morphology above the Paneth cell compartment is marked with an asterisk. (*G*) CBC cells differentiated along the Paneth cell lineage as marked by the appearance of small, electron-dense secretory granules. In (*G*), asterisks indicate the position of the intestinal lumen. [Scale bar: 10 μm (*D* and *E*); 2 μm (*F* and *G*).]

Musashi-1– and Dcamkl-1–positive cells (Fig. 3*G* and *H*). Taken together, the EM results confirm the observations that loss of epithelial cell proliferation causes premature differentiation of all progenitors as well as CBC cells, with the sole exception of cells residing immediately above the Paneth cell compartment.

Discussion

We describe a genetic model that provides a platform for selective disruption of cell division in any tissue of the adult mouse through targeted disruption of the CDC25 family of protein phosphatases. We focused on small intestinal epithelial cells in this study, because the major phenotype seen in these mice was a severe loss of absorptive surface of villi throughout the small intestine due to a loss of crypt epithelial cell proliferation. Expression of Cdc25-A, -B, and -C is enriched in crypts (Fig. S9). Intestinal epithelial cells are the fastest-proliferating cells in adult mice, followed by skin and blood cells (28, 29). Given that the TKO mice died within 1 week of *Cdc25A* disruption, it is not surprising that we found no phenotypes in other rapidly dividing mouse tissues.

Several conclusions can be drawn from our study in terms of the cell division cycle, the biology of small intestinal epithelial cells, and cancer therapy. With regard to cell cycle control, these conclusions include the following:

1. CDC25A is the only family member to provide an essential function during early embryonic development in mice. An essential role for one or more CDC25 families also has been found in fission yeast, worms, and flies (30–35).

2. Although CDC25A is essential during embryogenesis, a loss of CDC25A can be compensated for by other family members in adult mice.
3. Unlike in fission yeast, where Pyp3 can compensate for loss of CDC25 (36), the mammalian cell division cycle relies entirely on the CDC25 family to control cell division.
4. The small intestine phenotype described here is likely to be observed when adult mice are disrupted for other families of positive cell cycle regulators.

Current experimental models used to induce cell cycle arrest in the intestine include treatments that induce either DNA damage (radiation and chemotherapy) or tissue injury by dextran sulphate sodium (DSS) treatment (DSS) and genetic models that disrupt the Wnt or Notch signaling pathways. Here we report a novel model that directly targets the cell cycle engine to block cell division. A unique feature of this model is the maintenance of crypt depth, presumably due to the preservation of Wnt signaling (37, 38). Wnt signaling also is required to promote differentiation of progenitors along the secretory lineage (39, 40), and enhanced differentiation along this lineage was observed in the TKO mice (Fig. S10). Finally, Wnt signaling is required to maintain the self-renewal capacity of stem cells (24, 25, 41). The identity and location of intestinal epithelial stem cells remain unclear, due to the lack of clonogenic assays for validating candidate markers (42). Although our study does not definitively identify the small intestinal stem cells, our findings raise interesting questions as to their identity and how they respond to stress. Our data suggest that if CBC cells are indeed stem cells, then they respond to replication blocks and enhanced Wnt signaling by adopting the fate of neighboring cells, in this case by terminally differentiating into Paneth cells. In contrast, cells above the Paneth cell compartment underwent active Wnt signaling, as demonstrated by nuclear β catenin staining (Fig. 4*B*), yet they did not respond to these signals by differentiating like the CBC cells did. This failure to differentiate could be due to the fact that these cells are programmed to not differentiate in response to Wnt signaling and/or because they are more quiescent than other crypt cells (15–18). We are unable to distinguish between the role of Wnt signaling and quiescence, because Wnt signaling has critical stem cell nonautonomous effects in maintaining crypt architecture (37, 38). Thus, the inhibited proliferation in the absence of Wnt signaling results in crypt loss, and without crypts to house the stem cells, this implies that they too will be lost. The failure of cells residing immediately above the Paneth cell compartment to differentiate in response to Wnt signaling, coupled with their morphology by EM and their staining with Musashi-1 and Dcamkl-1, poses the question as to whether these are in fact small intestine epithelial stem cells.

Efforts are currently underway to develop CDC25 inhibitors that can be used to treat cancers that overproduce CDC25 family members (43). The cytotoxicity of CDC25 inhibition needs to be assessed before such inhibitors can proceed to the clinic. The targeted gene knockout studies reported here predict that drugs that inhibit 1 or 2 family members will be well tolerated in patients. Chemotherapy and radiation therapy indirectly inhibit cell division by inducing DNA damage. In contrast, the blocking of CDC25 function inhibits cell division directly by preventing activation of the cell cycle engine. In this case, Wnt signaling is enhanced, apoptosis is not induced, and the number and structure of crypts are maintained. This is in stark contrast to chemotherapy and irradiation, which have been shown to induce apoptosis and crypt loss. Our findings indicate that in the absence of proliferation during periods of genotoxic stress, Wnt signaling in the small intestines maintains crypt structure and possibly ensures stem cell preservation. The preservation of stem cells under conditions in which proliferation is blocked (as in, e.g., patients undergoing radiation or chemotherapy) would ensure that the small intestine is efficiently repopulated with epithelial cells during the recovery process. Thus, the development of Wnt agonists that specifically target intestinal stem cells, but not cancer cells, may be of therapeutic benefit, reducing the side effects of common cancer treatments.

Methods

4-Hydroxytamoxifen Administration. 4-Hydroxytamoxifen (OHT; Sigma H6278) was administered i.p. The OHT was dissolved in sunflower seed oil (Sigma) at a concentration of 25 mg/mL by sonication. The dissolved OHT was injected i.p. at a dose of 8 mg/25 g of body weight per day for 3 consecutive days. Injected mice were monitored daily. In some cases, the OHT was dissolved in ethanol, insoluble particulates were precipitated and discarded, and the supernatant was lyophilized and prepared as described above. Mice ranged in age from 2 to 3 months at the time of injection.

Immunohistochemistry. Mouse tissues were fixed in 10% neutrally buffered formalin overnight. Tissue sections were deparaffinized in xylene and then rehydrated in a series of alcohols and PBS. Endogenous peroxidase activity was removed by incubating the sections in 3% hydrogen peroxide in methanol for 10 min. Antigen retrieval was done by boiling the sections in 8.2 mM sodium citrate and 1.8 mM citric acid in PBS for Musashi-1 staining or in 10 mM sodium citrate (pH 6.0) for all other stainings for 20 min. Sections were blocked with 10% normal donkey serum, 10% normal goat serum, and 2% normal mouse serum (Musashi-1 staining) or with 3% BSA and 0.1% Triton X-100 in PBS (for all other stainings) and incubated with the following antibodies at room temperature for 1 h: Musashi-1 (Chemicon; 1:100), Dcamkl-1 (Santa Cruz Biotechnology; 1:100), geminin (Santa Cruz Biotechnology; 1:100), β-catenin (BD Transduction Laboratories; 1:100), L-Fabp (a gift from Dr. Jeff Gordon, Washington University; 1:100), Lysozyme (Dako Cytomation; 1:50), and BrdU (Serotec; 1:100). The following secondary antibodies were applied: anti-rabbit FITC (Jackson ImmunoResearch; 1:1000), anti-goat FITC (Jackson ImmunoResearch; 1:1000), anti-rabbit horseradish peroxidase (for geminin, Zymed; 1:1000), and anti-rat Cy5 (Jackson ImmunoResearch; 1:100). For geminin staining, the sections were incubated with FITC Plus (PerkinElmer; 1:50) for 30 min. For β-catenin staining, the MOM kit (Vector Laboratories) and fluorescein avidin D (Vector Laboratories; 1:1000) were used to block nonspecific binding of secondary antibodies. The sections were mounted with ProLong Gold antifade reagent with DAPI (Invitrogen). The sections were viewed using an Olympus BX60 microscope and a SPOT CCD camera (Diagnostic Instruments). Adobe Photoshop 7.0 was used to pseudocolor and overlap images obtained from different filter sets. For BrdU single staining, BrdU (Amersham) was injected i.p. according to the manufacturer's recommendations (2 mL/100 g of body weight). One hour later, the mice were euthanized, and their intestinal tracts were dissected and processed as described above. BrdU staining was performed with the Zymed BrdU staining kit according to the manufacturer's instructions.

Gastrointestinal Tract, Crypt, and Villi Measurements. Small and large intestines were isolated from the TKO and control mice 3 or 4 days after the final injection. The intestines were cut open along the cephalocaudal axis, pinned down on a solid plate, and fixed overnight with 10% neutrally buffered formalin. The small and large intestines were measured along their entire length and normalized with initial body weights. Villi at the most proximal end of the small intestine were used for length measurements. Cross-sections of duodenum were photographed under a dissection microscope, and the actual villus lengths were calculated using a scale bar provided in the same picture. A total of 30 villi per mouse were measured.

Transmission Electron Microscopy. Intestines were dissected and fixed in 2% paraformaldehyde/2.5% glutaraldehyde and embedded in Eponate 12 resin. Sections of 95 nm were obtained. These sections were stained with uranyl acetate and lead citrate and viewed on a JEOL 1200 EX transmission electron microscope.

ACKNOWLEDGMENTS. We thank Mike White for performing the blastocyst injections, Mark Watson for assisting with LCM, Janis Watkins and Shirong Cai for providing technical assistance, Dr. Anton Berns for providing the knock-in mice expressing CreER^T from the *Rosa26* locus, and Chris Ryan for editing the manuscript. We thank the Alvin J. Siteman Cancer Center at Washington University School of Medicine and Barnes-Jewish Hospital for the use of the Embryonic Stem Cell Core. The Siteman Cancer Center is supported in part by an NCI Cancer Center Support Grant (P30 CA91842). G. L. was supported in part by the Cancer Biology Pathway program administered through the Siteman Cancer Center. This work was supported by grants from the Pew Scholars Program in the Biomedical Sciences and the Crohn's Colitis Fund of America (to T.S.S.) and from the National Institutes of Health (to H.P.-W., who is an Investigator of the Howard Hughes Medical Institute).

1. Lee MS, et al. (1992) *Cdc25*$^{+}$ encodes a protein phosphatase that dephosphorylates p34cdc2. *Mol Biol Cell* 3:73–84.
2. Dunphy WG, Kumagai A (1991) The CDC25 protein contains an intrinsic phosphatase activity. *Cell* 67:189–196.
3. Gautier J, Solomon MJ, Booher RN, Bazan JF, Kirschner MW (1991) CDC25 is a specific tyrosine phosphatase that directly activates p34cdc2. *Cell* 67:197–211.
4. Sebastian B, Kakizuka A, Hunter T (1993) Cdc25M2 activation of cyclin-dependent kinases by dephosphorylation of threonine-14 and tyrosine-15. *Proc Natl Acad Sci U S A* 90:3521–3524.
5. Strausfeld U, et al. (1991) Dephosphorylation and activation of a p34cdc2/cyclin B complex in vitro by human CDC25 protein. *Nature* 351:242–245.
6. Honda R, Ohba Y, Nagata A, Okayama H, Yasuda H (1993) Dephosphorylation of human p34cdc2 kinase on both Thr-14 and Tyr-15 by human CDC25B phosphatase. *FEBS Lett* 318:331–334.
7. Kakizuka A, et al. (1992) A mouse CDC25 homolog is differentially and developmentally expressed. *Genes Dev* 6:578–590.
8. Nargi JL, Woodford-Thomas TA (1994) Cloning and characterization of a CDC25 phosphatase from mouse lymphocytes. *Immunogenetics* 39:99–108.
9. Wickramasinghe D, et al. (1995) Two CDC25 homologues are differentially expressed during mouse development. *Development* 121:2047–2056.
10. Wu S, Wolgemuth, DJ (1995) The distinct and developmentally regulated patterns of expression of members of the mouse *Cdc25* gene family suggest differential functions during gametogenesis. *Dev Biol* 170:195–206.
11. Chen M-S, Hurov J, White LS, Woodford-Thomas T, Piwnica-Worms H (2001) Absence of apparent phenotype in mice lacking CDC25C protein phosphatase. *Mol Cell Biol* 21:3853–3861.
12. Lincoln AJ, et al. (2002) CDC25B phosphatase is required for resumption of meiosis during oocyte maturation. *Nat Genet* 30:446–449.
13. Ferguson AM, White LS, Donovan PJ, Piwnica-Worms H (2005) Normal cell cycle and checkpoint responses in mice and cells lacking CDC25B and CDC25C protein phosphatases. *Mol Cell Biol* 25:2853–2860.
14. Radtke F, Clevers H (2005) Self-renewal and cancer of the gut: Two sides of a coin. *Science* 307:1904–1909.
15. Barker N, et al. (2007) Identification of stem cells in small intestine and colon by marker gene *Lgr5*. *Nature* 449:1003–1007.
16. Cheng H, Leblond CP (1974) Origin, differentiation and renewal of the four main epithelial cell types in the mouse small intestine, V: Unitarian theory of the origin of the four epithelial cell types. *Am J Anat* 141:537–561.
17. Marshman E, Booth C, Potten CS (2002) The intestinal epithelial stem cell. *Bioessays* 24:91–98.
18. Sangiorgi E, Capecchi MR (2008) Bmi1 is expressed in vivo in intestinal stem cells. *Nat Genet* 40:915–920.
19. Vooijs M, Jonkers J, Berns A (2001) A highly efficient ligand-regulated Cre recombinase mouse line shows that *LoxP* recombination is position-dependent. *EMBO Rep* 21:292–297.
20. McGarry TJ, Kirschner MW (1998) Geminin, an inhibitor of DNA replication, is degraded during mitosis. *Cell* 93:1043–1053.
21. Sweetser DA, Birkenmeier EH, Hoppe PC, McKeel DW, Gordon JI (1988) Mechanisms underlying generation of gradients in gene expression within the intestine: An analysis using transgenic mice containing fatty acid binding protein–human growth hormone fusion genes. *Genes Dev* 2:1318–1332.
22. Kayahara T, et al. (2003) Candidate markers for stem and early progenitor cells, Musashi-1 and Hes1, are expressed in crypt base columnar cells of mouse small intestine. *FEBS Lett* 535:131–135.
23. Giannakis M, et al. (2006) Molecular properties of adult mouse gastric and intestinal epithelial progenitors in their niches. *J Biol Chem* 281:11292–11300.
24. Gregorieff A, Clevers H (2005) Wnt signaling in the intestinal epithelium: From endoderm to cancer. *Genes Dev* 19:877–890.
25. Sancho E, Batlle E, Clevers H (2004) Signaling pathways in intestinal development and cancer. *Annu Rev Cell Dev Biol* 20:695–723.
26. van Es JH, et al. (2005) Wnt signaling induces maturation of Paneth cells in intestinal crypts. *Nat Cell Biol* 7:381–386.
27. el Marjou F, et al. (2004) Tissue-specific and inducible Cre-mediated recombination in the gut epithelium. *Genesis* 39:186–193.
28. Blanpain C, Horsley V, Fuchs E (2007) Epithelial stem cells: Turning over new leaves. *Cell* 128:445–458.
29. Cheshier SH, Morrison SJ, Liao X, Weissman IL (1999) In vivo proliferation and cell cycle kinetics of long-term self-renewing hematopoietic stem cells. *Proc Natl Acad Sci U S A* 96:3120–3125.
30. Russell P, Nurse P (1986) *Cdc25*$^{+}$ functions as an inducer in the mitotic control of fission yeast. *Cell* 45:145–153.
31. Fraser AG, et al. (2000) Functional genomic analysis of *C. elegans* chromosome I by systematic RNA interference. *Nature* 408:325–330.
32. Kamath RS, et al. (2003) Systematic functional analysis of the *Caenorhabditis elegans* genome using RNAi. *Nature* 421:231–237.
33. Alphey L, et al. (1992) Twine, a *Cdc25* homolog that functions in the male and female germline of *Drosophila*. *Cell* 69:977–988.
34. Edgar BA, O'Farrell PH (1989) Genetic control of cell division patterns in the *Drosophila* embryo. *Cell* 57:177–187.
35. Courtot C, Fankhauser C, Simanis V, Lehner CF (1992) The *Drosophila Cdc25* homolog twine is required for meiosis. *Development* 116:405–416.
36. Millar JB, Lenaers G, Russell P (1992) Pyp3 PTPase acts as a mitotic inducer in fission yeast. *EMBO J* 11:4933–4941.
37. Pinto D, Gregorieff A, Begthel H, Clevers H (2003) Canonical Wnt signals are essential for homeostasis of the intestinal epithelium. *Genes Dev* 17:1709–1713.
38. Kuhnert F, et al. (2004) Essential requirement for Wnt signaling in proliferation of adult small intestine and colon revealed by adenoviral expression of Dickkopf-1. *Proc Natl Acad Sci U S A* 101:266–271.
39. Sansom OJ, et al. (2004) Loss of Apc in vivo immediately perturbs Wnt signaling, differentiation, and migration. *Genes Dev* 18:1385–1390.
40. Andreu P, et al. (2005) Crypt-restricted proliferation and commitment to the Paneth cell lineage following Apc loss in the mouse intestine. *Development* 132:1443–1451.
41. Korinek V, et al. (1998) Depletion of epithelial stem cell compartments in the small intestine of mice lacking Tcf-4. *Nat Genet* 19:379–383.
42. Bjerknes M, Cheng H (2006) Intestinal epithelial stem cells and progenitors. *Methods Enzymol* 419:337–383.
43. Kristjansdottir K, Rudolph J (2004) CDC25 phosphatases and cancer. *Chem Biol* 11, 1043–1051.